Journal of Molecular Catalysis A: Chemical 313 (2009) 49–54

Contents lists available at ScienceDirect

Journal of Molecular Catalysis A: Chemical

journal homepage: www.elsevier.com/locate/molcata

A DFT study of the electronic structure of cobalt and nickel mono-substituted MoS_2 triangular nanosized clusters

Carolina Zuriaga-Monroy[a], José-Manuel Martínez-Magadán[b], Estrella Ramos[c], Rodolfo Gómez-Balderas[a,*]

[a] Laboratorio de Fisicoquímica Analítica, Unidad de Investigación Multidisciplinaria, FES Cuautitlán, Universidad Nacional Autónoma de México, Cuautitlán Izcalli, Estado de México, 54700, Mexico
[b] Programa de Ingeniería Molecular, Instituto Mexicano del Petróleo, Eje Central Lázaro Cárdenas Norte 152, San Bartolo Atepehuacán, México D. F. 07730, Mexico
[c] Instituto de Investigaciones en Materiales, Universidad Nacional Autónoma México, Ciudad Universitaria, México D. F. 04510, Mexico

ARTICLE INFO

Article history:
Received 5 December 2008
Received in revised form 29 July 2009
Accepted 3 August 2009
Available online 8 August 2009

Keywords:
HDS
Promoting effects
Molybdenum sulfide
Nanoparticle
DFT

ABSTRACT

Molybdenum disulfide nanoparticles are of interest for their extensive use in heterogeneous catalysis. Here, we report a systematic density functional theory study carried out to investigate the electronic effects of Co(Ni) mono-substitutions on triangular molybdenum sulfide models of nanometric scale. On the basis of the electronic structure, the charge distribution and the $\Delta(E_{LUMO} - E_{HOMO})$ gap analysis, the triangle molecular model with nickel substitution is identified as more favorable for inducing the best catalytic performance. Nickel consistently induces stronger electronic rearrangements than cobalt, on the molybdenum first-neighbor atoms, which are connected with its higher promoting effect. Charge distribution analysis points out a chemical reduction on the molybdenum sites when the cluster is doped. Moreover, nickel substitution produces smaller $\Delta(E_{LUMO} - E_{HOMO})$ gaps than cobalt substitutions, revealing that Ni-doped clusters are more reactive.

1. Introduction

In recent years environmental regulations have resulted in the demand for ultralow sulfur transport fuels, this fact drives the continuous research and development of new hydrotreating catalysts with higher activity and selectivity. Molybdenum sulfides based catalysts, supported on alumina (MoS_2/Al_2O_3), have been widely used in hydrotreating processes, mainly in the hydrogenation of aromatic compounds and the hydrogenolysis of sulfur from organic compounds present in petroleum (hydrodesulfurization, HDS) [1]. The incorporation of cobalt and nickel into molybdenum sulfides produces promoted catalysts ($Co(Ni)/MoS_2$), that show much higher activities than the corresponding monometallic molybdenum, cobalt or nickel sulfides [1,2].

In order to obtain a detailed description of the role of the catalyst during desulfurization, many aspects of ($Co(Ni)/MoS_2$) structure, properties and activity have been studied from both experimental and theoretical views, useful reviews have been published [3–5]. Key findings were derived from extended X-ray absorption fine structure EXAFS [6–10], Mössbauer emission spectroscopy [11] and IR techniques [12,13], which allowed to identify a Co–Mo–S type structure as the active phase responsible for the promoting effects during the HDS. From these results emerged the view that the Co–Mo–S (and Ni–Mo–S) structures are small MoS_2-like crystallites [14], where promoter atoms decorate the edges of the MoS_2 catalyst and constitutes the active sites.

In the active catalyst, metal centers located at the edges of MoS_2 particles have a local stoichiometry and structure that differs from the catalytically inert basal planes. It has been suggested that Co atoms are located in the Mo plane, likely showing a local coordination different from that of molybdenum in the pure MoS_2. Density functional theory (DFT) simulations have demonstrated that Co and Ni indeed substitutes Mo at the S- or Mo-edge [15] modifying the electronic structure of Mo sites [16].

It has been documented that materials fragmented down to nanoparticles may display new and interesting electronic, as well as structural, features that differ from those exhibited by the bulk system [17]. As a consequence of the new electronic characteristics nanoparticles may adopt unique catalytic properties. Recently, MoS_2 nanoparticles were synthesized in ultrahigh vacuum conditions on Au(1 1 1) nanotemplates, by using scanning tunneling microscopy (STM) atomic resolved structures of unpromoted and promoted MoS_2 have been obtained [18–21]. STM experiments have shown that umpromoted MoS_2 particles take a distinct triangular morphology. Whereas the presence of

* Corresponding author. Tel.: +52 55 5623 1999x39420; fax: +52 55 5870 5668.
E-mail address: gomezr@gmail.com (R. Gómez-Balderas).

1381-1169/$ – see front matter © 2009 Elsevier B.V. All rights reserved.
doi:10.1016/j.molcata.2009.08.001

the Co(Ni) promoter implies changes in the morphology of the clusters, Co(Ni)MoS nano-crystallites are closer to a hexagonal shape [22]. Furthermore, STM images have made possible to elucidate the catalytically important edges, estimate the sulfur coverage and the location of sulfur vacancies (coordinatively unsaturated sites, CUS) which are proposed to be the HDS active sites [18].

Despite the many proposals, based on experimental and theoretical approaches, about the nature of the promoting effects, a clear view has not yet been achieved. DFT studies on structural models can be employed to discuss the promoter effects, in terms of the electronic structure of the systems. In the present study we have used density functional theory to investigate the effect of the promoters, cobalt or nickel, on the electronic structure of MoS_2 triangular nanoclusters (Fig. 1). The projected density of states on the atomic sites is analyzed to explore the changes induced by a promoter atom on the Mo first-neighbor sites. Frontier orbital energies of the nanoparticle are also influenced by the presence of cobalt or nickel, thus the analysis of the HOMO–LUMO gap might provide information on the changes in the reactivity of the nanoparticles. Therefore, the catalytic activity of the Co(Ni)/MoS_2 particles can be discussed in relation with these electronic properties, as well as by examining the projected charges on the metal atomic sites, in particular the Hirshfeld partitioning scheme has been employed here for a qualitative analysis, on the influence of the promoters on the molybdenum sites, that should be interpreted in the context of the whole electronic structure features.

2. Computational methods

2.1. Nanoparticle models

MoS_2 nanosize particles, synthesized in ultrahigh vacuum conditions on gold nanotemplates, have been reported to be almost exclusively triangular in shape. For small clusters, the triangles with $n = 4$ or 5 are preferred, n being the number of Mo atoms per side in the cluster [20]. The nanoparticle models used here for the pure system were built up from a S–Mo–S sheet, taking a triangle of 1.58 nm per side with $n = 5$ ($Mo_{15}S_{42}$ stoichiometry) Fig. 1.

As it has been discussed, the presence of promoters implies changes in the morphology of the cluster, being the CoMoS closer to a hexagonal nano-crystallites [22,23]. The focus here is the effect of Co(Ni) mono-substitutions of Mo, therefore the triangular shape model will be employed all along this work. A hexagonal morphology might be considered for models with more substitutions at the edge, however. To model the doped systems each Mo position in the pure cluster was replaced by a Co(Ni) atom at the time, followed by geometry optimization. Given the pure cluster symmetry prior to optimization, there are just four different positions where Co(Ni) can replace Mo in a mono-substitution fashion (see Fig. 1). The Co- and Ni-doped systems have the stoichiometry $CoMo_{14}S_{42}$ and $NiMo_{14}S_{42}$, respectively.

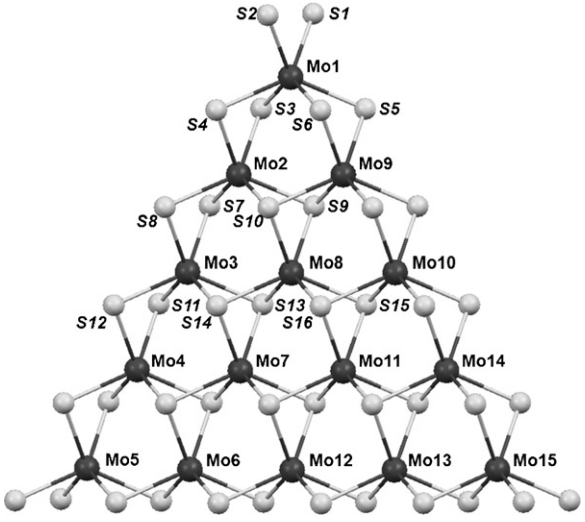

Fig. 1. $Mo_{15}S_{42}$ nanoparticule model. Molybdenum can be substituted by cobalt or nickel at the Mo1 (Co(Ni)@1$Mo_{14}S_{42}$), Mo2 (Co(Ni)@2$Mo_{14}S_{42}$), Mo3 (Co(Ni)@3$Mo_{14}S_{42}$) and Mo8 (Co(Ni)@8$Mo_{14}S_{42}$) sites.

Calculations were run using the supercell approximation ($A = B = 22.162$ and $C = 12.275$ Å, $\alpha = \beta = 90^\circ$ and $\gamma = 120^\circ$), each cluster was placed in a supercell large enough to allow for an initial 6.332 Å distance between periodic replica, this precaution avoids spurious interactions between atoms belonging to vicinal cells due to the periodic boundary conditions imposed for the calculations. It has been reported that the maximum activities of Co(Ni)/MoS_2 catalysis are obtained at a Co(Ni)/[Co(Ni) + Mo] ratio close to 0.3, to reach this ratio a model with four doping atoms would be needed, with a mono-substitution scheme the ratio is close to 0.07.

2.2. Density functional theory calculations

Density functional theory (DFT) has been used to determine the geometry and electronic structure of pure, Co- and Ni-doped MoS_2 nanometric models. *Ab initio* computations were carried out using DFT in the generalized gradient approximation (GGA) with the Materials Studio DMol^3 program [24,25] from Accelrys Inc. We employed the revised Perdew–Burke–Ernzerhof (RPBE) exchange-correlation functional [26] with a double numerical plus polarization functions basis set (DNP) to describe the valence electrons, in combination with Hartree-Fock effective core potentials [27,28] for the treatment of the ionic cores. The used real space radii are 4.0, 4.9 and 4.5 Å for sulfur, molybdenum and cobalt(nickel) atoms, respectively. All the systems were relaxed until the remaining total force was below 0.002 Ha/Å, a thermal smearing of 0.05 Ha was used for geometry optimization. For calculating the electronic properties, a more stringent smearing of 0.003 Ha was used to set the orbital occupancy. Spin polarization scheme was applied to all calculations.

3. Results and discussion

3.1. Geometry optimization

Selected metal–sulfur distances, after geometry optimization, are collected in Table 1. We can compare the distances metal–sulfur, in the Mo, Co and Ni coordination spheres, in positions of interest in the pure and doped nanoclusters. Distances in the coordination spheres are shorter for the more exposed sulfurs (edges and corners) than those for the more inner ones. In general, substitution decreases the distance of the more exposed S while increases that of the internal sulfurs; nickel produces bigger changes than cobalt. When substitution is done at the center of the particle (Mo8 site) practically there is no change for nickel, while cobalt produces only a small length reduction. Recent DFT calculations, on the intrinsic properties of MoS_2 triangular sulfur terminated nanoclusters, have proven that the two outermost sulfur atoms are found to contract in the direction perpendicular to the basal plane forming sulfur dimers [20], whereas the length of the core atoms remain practically unchanged relative to the corresponding ones in the bulk [29]. It seems promoter atoms contribute in the same sense; substitution at Mo1, Mo2 and Mo3 sites shorten the S–S distances with respect to the pure system, this fact might help in forming sulfur vacancies.

Table 1
Optimized structure bond lengths (Å) for pure and doped systems. For the doped systems bond lengths in the metal coordination sphere are in bold.

	$Mo_{15}S_{42}$	Co@1	Ni@1	Co@2	Ni@2	Co@3	Ni@3	Co@8	Ni@8
Mo1S1	2.556	**2.475**	**2.479**	2.544	2.545	2.554	2.553	2.557	2.557
Mo1S2	2.556	**2.475**	**2.479**	2.544	2.545	2.554	2.554	2.557	2.557
Mo1S3	2.615	**2.635**	**2.682**	2.616	2.605	2.615	2.614	2.614	2.616
Mo1S4	2.615	**2.635**	**2.682**	2.616	2.605	2.615	2.614	2.614	2.615
Mo1S5	2.613	**2.635**	**2.682**	2.614	2.620	2.614	2.614	2.616	2.618
Mo1S6	2.612	**2.635**	**2.682**	2.614	2.620	2.614	2.614	2.616	2.618
Mo2S3	2.597	2.584	2.581	**2.534**	**2.573**	2.588	2.587	2.595	2.591
Mo2S4	2.597	2.584	2.581	**2.534**	**2.573**	2.588	2.587	2.595	2.591
Mo2S7	2.602	2.593	2.592	**2.529**	**2.576**	2.593	2.593	2.602	2.607
Mo2S8	2.602	2.593	2.592	**2.529**	**2.576**	2.593	2.593	2.602	2.607
Mo2S9	2.633	2.640	2.642	**2.766**	**2.729**	2.639	2.641	2.624	2.626
Mo2S10	2.633	2.640	2.642	**2.766**	**2.729**	2.639	2.641	2.624	2.627
Mo3S7	2.602	2.603	2.603	2.601	2.593	**2.565**	**2.581**	2.604	2.608
Mo3S8	2.602	2.603	2.603	2.601	2.593	**2.565**	**2.581**	2.604	2.608
Mo3S11	2.602	2.603	2.603	2.592	2.593	**2.564**	**2.580**	2.599	2.595
Mo3S12	2.602	2.603	2.603	2.592	2.593	**2.564**	**2.580**	2.599	2.595
Mo3S13	2.636	2.637	2.636	2.636	2.643	**2.679**	**2.729**	2.624	2.627
Mo3S14	2.636	2.637	2.636	2.636	2.643	**2.679**	**2.729**	2.624	2.627
Mo7S9	2.623	2.622	2.623	2.610	2.611	2.627	2.629	**2.602**	**2.621**
Mo7S10	2.623	2.622	2.623	2.610	2.611	2.627	2.629	**2.602**	**2.621**
Mo7S13	2.625	2.625	2.625	2.628	2.630	2.617	2.615	**2.605**	**2.626**
Mo7S14	2.625	2.625	2.625	2.628	2.630	2.617	2.615	**2.605**	**2.626**
Mo7S15	2.624	2.625	2.625	2.619	2.616	2.618	2.617	**2.605**	**2.626**
Mo7S16	2.624	2.625	2.625	2.619	2.616	2.618	2.617	**2.605**	**2.626**
S1S2	3.293	3.275	3.347	3.313	3.314	3.392	3.293	3.298	3.290
S3S4	3.229	3.164	3.172	3.166	3.185	3.241	3.243	3.237	3.240
S5S6	3.229	3.164	3.172	3.212	3.215	3.231	3.232	3.234	3.238
S7S8	3.238	3.249	3.252	3.188	3.205	3.182	3.195	3.231	3.221
S9S10	3.276	3.264	3.259	3.200	3.199	3.263	3.258	3.210	3.218
S11S12	3.238	3.239	3.241	3.247	3.252	3.188	3.202	3.245	3.247
S13S14	3.283	3.284	3.284	3.265	3.263	3.204	3.205	3.216	3.224
S15S16	3.283	3.284	3.284	3.292	3.287	3.288	3.287	3.219	3.227

3.2. Pure $Mo_{15}S_{42}$ nanoparticles

Comparing the *d*-projected density of states (DOS) as a function of the energy onto the metal sites, is useful to detect and analyze the repositioning of the electronic states, in particular around the Fermi level where the chemical reactivity features can be explored. The upper panel of Fig. 2 shows the total *d*-projected density of states for the pure nanoparticle model, this nanoparticle has a metallic character, exhibiting electronic properties different from its bulk counterpart, a semiconductor with an indirect band gap. In agreement with Ref. [30], we observe a minimum in the DOS at the Fermi level.

Fig. 2 also depicts the *d*-projected density of states for the molybdenum sites, we can observe that the density of unoccupied states, near the Fermi level, is decreased as we go from the corner site (Mo1) to the core site (Mo8), while the density of the occupied states just below the Fermi level is increased, the edge positions (Mo2 and Mo3) represent an intermediate situation. The high density of unoccupied states makes Mo1 more capable for accepting electrons.

3.3. Co(Ni)$Mo_{14}S_{42}$ nanoparticles

Fig. 3 displays the *d* density of states for the nanoparticle model with Mo substituted by Co(Ni) at the position Mo1 (Co(Ni)@1$Mo_{14}S_{42}$), see upper panel. At this position, density of states of cobalt and nickel are higher than molybdenum above the Fermi level; an interesting feature is that the maximum for the density of unoccupied states of nickel is closer to the Fermi level than cobalt; this fact would enhance the acceptor capability of the cluster by the presence of nickel. On the other hand, cobalt shows a peak of DOS just below the Fermi level, which in turn might indicate improvement of donating capability of the cluster by the influence of cobalt. By the influence of the promoter, the density

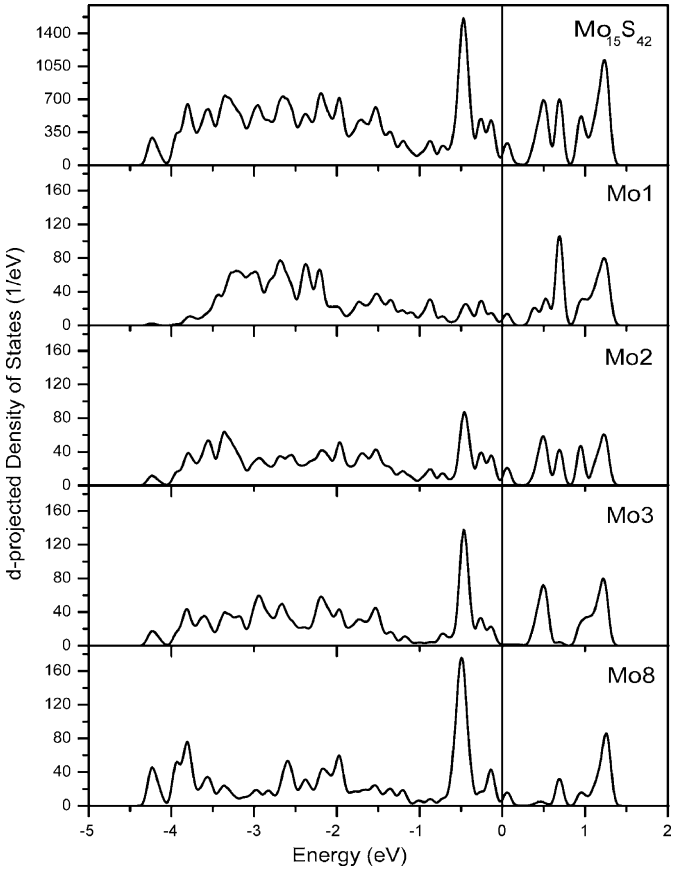

Fig. 2. *d*-Projected density of states on the molybdenum sites in the $Mo_{15}S_{42}$ nanoparticle.

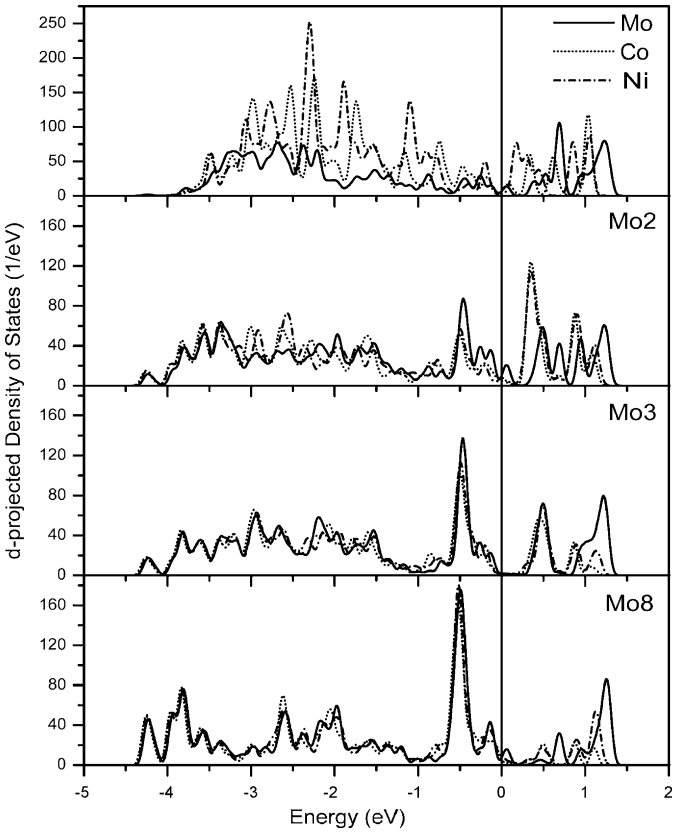

Fig. 3. *d*-Projected density of states on the metal sites in the Co(Ni)@1$Mo_{14}S_{42}$ nanoparticle. The first panel displays the Mo1 and Co(Ni)@1 for the pure and doped systems, respectively.

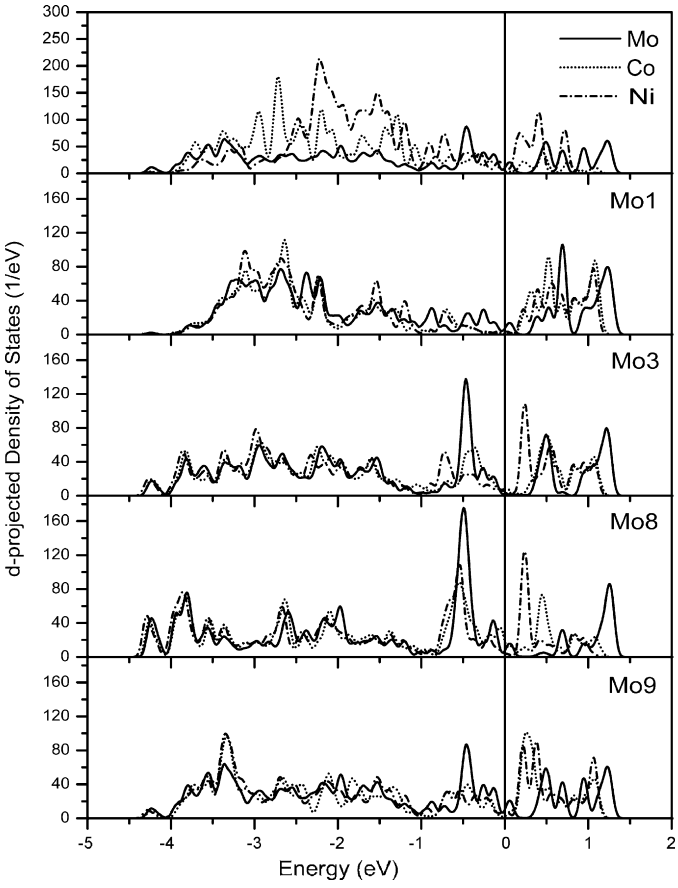

Fig. 4. *d*-Projected density of states on the metal sites in the Co(Ni)@2$Mo_{14}S_{42}$ nanoparticle. The upper panel shows the Mo2 and Co(Ni)@2 for the pure and doped systems, respectively.

of unoccupied states above the Fermi level of the Mo2 is increased. The molybdenum DOS at the positions Mo3 and Mo8, far from the doping site, shows just small rearrangements due to the promoters.

Promoting the $Mo_{15}S_{42}$ cluster at the Mo2 position (Co(Ni)@$2Mo_{14}S_{42}$) produces more noticeable perturbations in all the molybdenum first-neighbor sites. The first panel in the Fig. 4 displays the DOS at the Mo2 position; the DOS of Ni in the unoccupied region is higher than Mo and Co. In all the positions, nickel modifies the DOS of molybdenum displacing the maxima of the unoccupied states towards the Fermi level; in contrast cobalt produces smaller changes. On the other hand, the densities of occupied states are reduced by the presence of doping atoms at all the Mo sites.

When the promoter atom is placed at the Mo3 position (Co(Ni)@3$Mo_{14}S_{42}$), we observe the more significant rearrangements of the electronic states (Fig. 5). Molybdenum unoccupied states are shifted towards the Fermi level, with an appreciable peak appearing when the doping is nickel. Even in the core molybdenum sites this effect can be observed, for both Co and Ni. In contrast occupied states are diminished by the promoter, compared with the pure $Mo_{15}S_{42}$ nanoparticle.

Finally, Fig. 6 shows the *d*-projected DOS for the doped cluster at the position Mo8 (Co(Ni)@8$Mo_{14}S_{42}$). This is a core position which in principle is expected to have a modest participation in the catalysis. Co as well as Ni atomic sites, at the Mo8 position, present high density of unoccupied states just above the Fermi level. The Mo2 and Mo3 positions, both edge positions, displays high density of unoccupied states closer to the Fermi level, which takes the place of the valley present in the DOS of the corresponding Mo2 and Mo3 in the pure system. In contrast, there is a depletion of the density of occupied states due to the promoter. States from cobalt and nickel are clearly displayed in the Mo7 position at the Fermi level.

3.4. Frontier orbital energies

The gap in energy between the HOMO and LUMO is an important chemical reactivity index; a large gap indicates high stability and a small gap low stability. In turn, the high stability is associated with low chemical reactivity and the small stability with high chemical reactivity [30–32]. It is well known that DFT underestimates the band gaps, and so is expected for the $\Delta(E_{LUMO} - E_{HOMO})$, therefore all the computations here will present this error. For instance, the calculated band gap for the MoS_2 bulk at the same level of theory gives 0.9 eV, smaller than the experimental of 1.4 eV. However, comparison of calculated $\Delta(E_{LUMO} - E_{HOMO})$ gaps between systems, is yet valuable in order to recognize trends. Table 2 reports the eigenvalues of the HOMO (E_{HOMO}), LUMO (E_{LUMO}) and the difference in energy between LUMO and HOMO $\Delta(E_{LUMO} - E_{HOMO})$ orbitals for the nanoparticles, we can see that all the doped clusters show smaller gaps than the pure system (0.065 eV), cobalt ranging from 0.017 to 0.024 eV and Ni from 0.005 to 0.14 eV. The gaps of the nickel systems are consistently narrower than the corresponding cobalt systems. This fact points out that Ni performs better in promoting the cluster reactivity than cobalt does. Aside the Mo8 positions, promoters in the corner position prone the cluster to a higher reactivity.

3.5. Hirshfeld charge analysis

The charge calculation was done using the Hirshfeld partitioning sheme [33]. In Table 3, we can observe that in general promoters donate charge to molybdenum first-neighbors making Mo sites more negative than the pure nanocluster. For instance, when Mo1 is

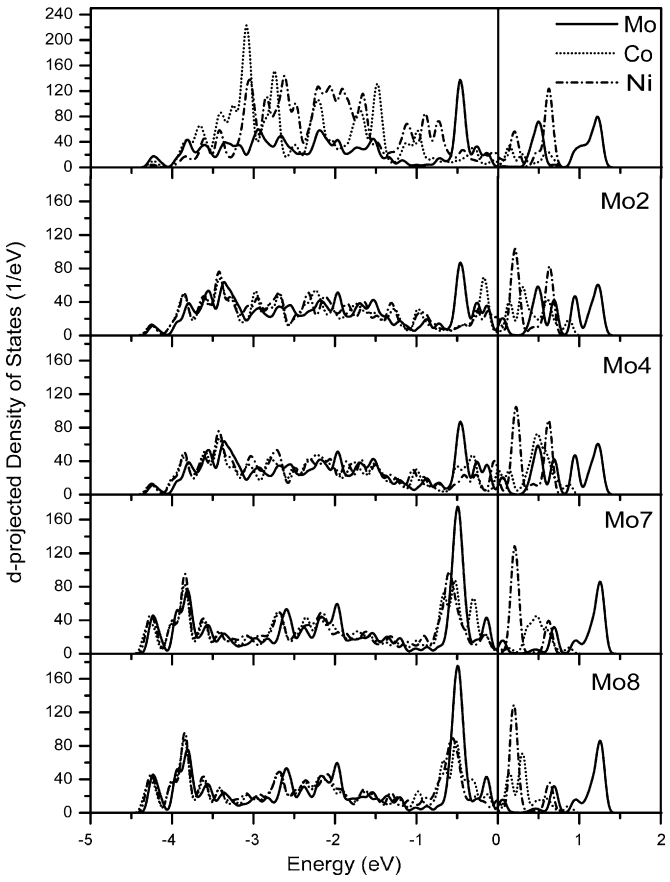

Fig. 5. *d*-Projected density of states on the metal sites in the Co(Ni)@3$Mo_{14}S_{42}$ nanoparticle. The upper panel displays the Mo3 and Co(Ni)@3 for the pure and doped clusters, respectively.

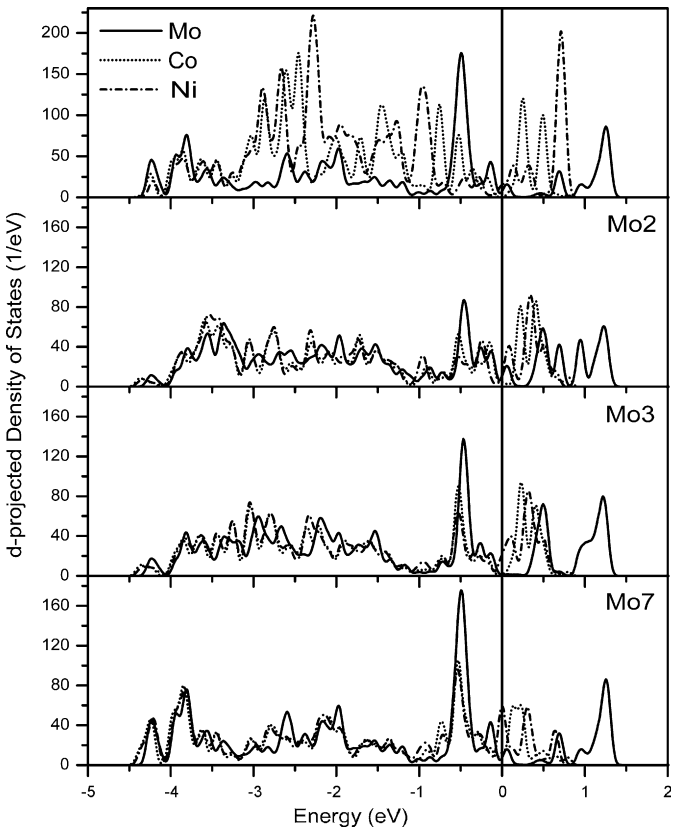

Fig. 6. *d*-Projected density of states on the metal sites in the Co(Ni)@8$Mo_{14}S_{42}$ nanoparticle. The top panel shows the Mo8 and Co(Ni)@8 for the pure and doped systems, respectively.

substituted by Co and Ni, the negative charge on the first-neighbor Mo2 atoms goes from −0.319 to −0.346 and −0.348, respectively. When promoter is placed at the Mo2 position, the charge in the corner site (Mo1) goes from −0.354 to −0.383 and −0.384, for Co and Ni respectively. For the same cluster, the charge in the edge site Mo3 is also more negative under the influence of Co and Ni, changing from −0.317 to −0.339 and −0.350. This electron donation will result in a formal oxidation of Co or Ni and a chemical reduction of Mo. This fact has been rationalized as a consequence of orbital interactions, the Mo 4d t_{2g} orbital, lying between the Co(Ni) e_g and t_{2g} orbitals, accommodates the 3d electrons from partially occupied orbitals of Co(Ni) [3]. We can also realize that comparing two equivalent first-neighbor molybdenum sites of nanocluster doped with Co and Ni in the same position, the one promoted with Ni is in general more reduced than the one doped with Co. See for example the Mo2 position in the Co(Ni)@3$Mo_{14}S_{42}$, where charge goes from −0.319 to −0.345 and −0.350 for Co and Ni, respectively.

3.6. Implications for the HDS catalysis

Catalytic activity for the C–S breaking in the HDS process has been proposed to follow a donation–back-donation electron mechanism. Electrons are donated from the sulfide molecule towards the d orbitals of the metal site, and then charge is back-donated from the occupied metal orbitals to the molecule antibonding π* C–S states [34–36]. Thus, a high density of states just below the Fermi level are responsible of the metallic character of the metal site and are at the origin of the back-donation into the π* antibonding orbital. On the other hand, a peak just above the Fermi level will be related with the acceptor properties of the atomic site playing a role in the donation step. This feature is clearly responsible for the strong adsorption energies of the sulfur atoms and sulfide molecules. Experimental measurements have shown that the promotion of MoS_2 with Ni enhances bonding interactions with thiophene, a typical test molecule in HDS [37].

From the results we can realize that Co and Ni shift the Mo unoccupied band towards the Fermi level, making more favorable the participation of molybdenum first-neighbor site in the donation of charge from the sulfide molecule, in the HDS process. Due to the features of our model, the *d*-projected density of states reflects the capability of the saturated metal sites to participate in the adsorption of the organic species and in certain way in the C–S bond breaking. But, because of the absence of CUS in the nanoparticles studied here, the states responsible of the back-donation are diminished, as we can see on the DOS below the Fermi level (see for instance Fig. 4). In fact, STM experiments reveal that transformation of thiophene into butenethiol may occur on the metallic sites

Table 2
Energies (eV) of the HOMO, LUMO and energy gaps for the pure and doped nanoparticles.

Nanocluster	E_{LUMO}	E_{HOMO}	$\Delta(E_{LUMO} - E_{HOMO})$
$Mo_{15}S_{42}$	−6.086	−6.151	0.065
Co@1$Mo_{14}S_{42}$	−6.134	−6.158	0.024
Co@2$Mo_{14}S_{42}$	−6.103	−6.152	0.049
Co@3$Mo_{14}S_{42}$	−6.134	−6.185	0.051
Co@8$Mo_{14}S_{42}$	−6.112	−6.129	0.017
Ni@1$Mo_{14}S_{42}$	−6.125	−6.138	0.014
Ni@2$Mo_{14}S_{42}$	−6.124	−6.147	0.023
Ni@3$Mo_{14}S_{42}$	−6.128	−6.145	0.017
Ni@8$Mo_{14}S_{42}$	−6.110	−6.116	0.005

Table 3
Calculated Hirshfeld atomic charges projected onto the metal sites. For the doped systems, charges on the first-neighbor metal sites are in bold.

Metal site	$Mo_{15}S_{42}$	Co@1	Ni@1	Co@2	Ni@2	Co@3	Ni@3	Co@8	Ni@8
Mo1	−0.354	−0.017	0.016	**−0.383**	**−0.384**	−0.353	−0.353	−0.351	−0.348
Mo2	−0.319	**−0.346**	**−0.348**	−0.043	−0.004	**−0.345**	**−0.350**	**−0.343**	**−0.346**
Mo3	−0.317	−0.319	−0.317	**−0.339**	**−0.350**	−0.050	−0.026	**−0.348**	**−0.350**
Mo4	−0.320	−0.320	−0.319	−0.318	−0.320	**−0.344**	**−0.352**	−0.320	−0.319
Mo5	−0.354	−0.354	−0.354	−0.354	−0.354	−0.356	−0.354	−0.354	−0.354
Mo6	−0.319	−0.319	−0.320	−0.319	−0.319	−0.318	−0.318	−0.319	−0.319
Mo7	−0.271	−0.270	−0.270	−0.268	−0.269	**−0.291**	**−0.303**	**−0.297**	**−0.297**
Mo8	−0.271	−0.269	−0.269	**−0.296**	**−0.300**	**−0.297**	**−0.303**	−0.002	−0.003
Mo9	−0.319	**−0.344**	**−0.348**	**−0.352**	**−0.352**	−0.317	−0.316	**−0.343**	**−0.347**
Mo10	−0.317	−0.318	−0.318	−0.320	−0.318	−0.318	−0.317	**−0.349**	**−0.350**
Mo11	−0.271	−0.270	−0.269	−0.269	−0.269	−0.267	−0.268	**−0.297**	**−0.296**
Mo12	−0.317	−0.317	−0.318	−0.317	−0.317	−0.318	−0.318	−0.316	−0.315
Mo13	−0.319	−0.319	−0.320	−0.319	−0.320	−0.320	−0.321	−0.319	−0.319
Mo14	−0.320	−0.320	−0.320	−0.320	−0.320	−0.321	−0.319	−0.320	−0.319
Mo15	−0.354	−0.354	−0.352	−0.354	−0.354	−0.353	−0.355	−0.354	−0.355

of the basal plane close to the edge, in the absence of CUS [20,38]. This fact would be favored by the unoccupied states of Mo8, when substitution occurs in Mo2 or Mo3 sites, and even when the promoter lay at the Mo8 position itself. However, to obtain the fully desulfirized product after the butenethiol formation, the existence of CUS is required at least for the second C–S bond breaking [4].

4. Conclusions

Simple model calculations prove to be useful in describing promotional effects of Co(Ni) on increasing reactivity of a series of mono-substitute $Mo_{15}S_{42}$ nanoclusters. DOS and band gaps show that nickel substitutions are more active than cobalt in modifying the electronic properties of the clusters. In connection with the donation–back-donation HDS mechanism, and due to the lack of CUS, promotional effect is observed as an increase of DOS above the Fermi level favoring the donation step; nevertheless, DOS below the Fermi level is diminished given no states available for the back-donation stage. Thus, the sulfur molecules will be preferably adsorbed on the cluster surface. Hirshfeld charges distribution points out the chemical reduction on the molybdenum sites for the doped clusters.

Acknowledgments

C.Z.-M. and R.G.-B. gratefully acknowledge generous allocations of computing time on the Kanbalam supercomputer of the Universidad Nacional Autónoma de México. This work is partially supported by the FES-C under grant PACIVE CONS100. E.R. thanks for the technical support of LI Victor Gomez, in the computer equipment of the IIM.

References

[1] H. Topsøe, B.S. Clausen, F.E. Massoth, in: J.R. Anderson, M. Bourdart (Eds.), Hydrotreating Catalysis Science and Technology, Springer-Verlag, Berlin/New York, 1996.
[2] R. Prins, V.H.J. de Beer, G.A. Somorjai, Catal. Rev.-Sci. Eng. 31 (1989) 1.
[3] R.R. Chianelli, G. Berhault, P. Raybaud, S. Kasztelan, J. Hafner, H. Toulhoat, Appl. Catal. A 227 (2002) 83.
[4] P. Raybaud, Appl. Catal. A 322 (2007) 76.
[5] M. Sun, J. Adjaye, A.E. Nelson, Appl. Catal. A 263 (2004) 131.
[6] B.S. Clausen, H. Topsøe, R. Candia, J. Villadsen, B. Lengeler, J. Als-Nielsen, F. Christensen, J. Phys. Chem. 85 (1981) 3868.
[7] B.S. Clausen, H. Topsøe, Hyperfine Interact. 47 (1989) 203.
[8] S.M.A.M. Bouwens, R. Prins, V.H.J. de Beer, D.C. Koningsberger, J. Phys. Chem. 94 (1990) 3711.
[9] C. Calais, N. Matsubayashi, C. Geantet, Y. Yoshimura, H. Shinada, A. Nishijima, M. Lacroix, M. Breysse, J. Catal. 174 (1998) 130.
[10] T. Shido, R. Prins, J. Phys. Chem. 102 (1998) 8426.
[11] J. Wivel, R. Candia, B. Clausen, S. Mørup, H. Topsøe, J. Catal. 68 (1981) 453.
[12] N.-Y. Topsøe, H. Topsøe, J. Catal. 84 (1983) 561.
[13] F. Maugé, J.C. Duchet, J.C. Lavalley, S. Houssenbay, E. Payen, J. Grimblot, S. Kasztelan, Catal. Today 10 (1991) 561.
[14] A.N. Startsev, Catal. Rev.-Sci. Eng. 37 (1995) 353.
[15] P. Raybaud, J. Hafner, G. Kresse, S. Kasztelan, H. Toulhoat, J. Catal. 190 (2000) 128.
[16] R. Gómez-Balderas, J.M. Martínez-Magadán, R. Santamaría, C. Amador, Int. J. Quantum Chem. 80 (2000) 406.
[17] U. Heiz, U. Landman (Eds.), Nanocatalysis, Springer, Berlin, 2007.
[18] S. Helveg, J.V. Lauritsen, E. Lægsgaard, I. Stensgaard, J.K. Nørskov, B.S. Clausen, H. Topsoe, F. Besenbacher, Phys. Rev. Lett. 84 (2000) 951.
[19] J.V. Lauritsen, S. Helveg, E. Lægsgaard, I. Stensgaard, B.S. Clausen, H. Topsøe, F. Besenbacher, J. Catal. 197 (2001) 1.
[20] J.V. Lauritsen, J. Kibsgaard, S. Helveg, H. Topsøe, B.S. Clausen, E. Lægsgaard, F. Besenbacher, Nat. Nanotechnol. 2 (2007) 53.
[21] J.V. Lauritsen, M. Nyberg, R.T. Vang, M.V. Bollinger, B.S. Clausen, H. Topsøe, K.W. Jacobsen, E. Lægsgaard, J.K. Nørskov, F. Besenbacher, Nanotechnology 14 (2003) 385.
[22] M. Brorson, A. Carlsson, H. Topsøe, Catal. Today 123 (2007) 31.
[23] J.V. Lauritsen, J. Kibsgaard, G.H. Olesen, P.G. Moses, B. Hinnemann, S. Helveg, J.K. Nørskov, B.S. Clausen, H. Topsøe, E. Lægsgaard, F. Besenbacher, J. Catal. 249 (2007) 220.
[24] B. Delley, J. Chem. Phys. 92 (1990) 508.
[25] B. Delley, J. Chem. Phys. 113 (2000) 7756.
[26] (a) L. Hammer, L.B. Hansen, J.K. Nørskov, Phys. Rev. B 59 (1999) 7413;
(b) The RPBE functional is the revised J.P. Perdew, K. Burke, M. Ernzerhof, Phys. Rev. Lett. 77 (1996) 3865;
(c) Independent to the previous revPBE proposed by Zhang, Yang, Phys. Rev. Lett. 80 (1998) 890.
[27] M. Dolg, U. Wedig, H. Stoll, H. Preuss, J. Chem. Phys. 86 (1987) 866.
[28] A. Bergner, M. Dolg, W. Kuechle, H. Stoll, H. Preuss, Mol. Phys. 80 (1993) 1431.
[29] T. Li, G. Galli, J. Phys. Chem. C 111 (2007) 16192.
[30] R.G. Pearson, J. Org. Chem. 54 (1989) 1423.
[31] Z. Zhou, R.G. Parr, J. Am. Chem. Soc. 112 (1990) 5720.
[32] W.L. Faust, Science 245 (1989) 37.
[33] F.L. Hirshfeld, Theor. Chim. Acta 44 (1977) 129.
[34] M.C. Zonnevylle, R. Hoffmann, S. Harris, Surf. Sci. 199 (1988) 320.
[35] J.A. Rodriguez, J. Phys. Chem. 101 (1997) 7524.
[36] R. Gómez-Balderas, R. Oviedo-Roa, J.M. Martínez-Magadán, C. Amador, D.A. Dixon, Surf. Sci. 518 (2002) 163.
[37] J.A. Rodriguez, J. Dvorak, A.M. Gabelnick, A.T. Capitano, J.L. Gland, Surf. Sci. 429 (1999) L462–L468.
[38] J.V. Lauritsen, M. Nyberg, J.K. Nørskov, B.S. Clausen, H. Topsøe, E. Lægsgaard, F. Besenbacher, J. Catal. 224 (2004) 94.